Recruitment of CTCF to an *Fto* enhancer is responsible for transgenerational inheritance of BPA-induced obesity

Yoon Hee Jung[1], Hsiao-Lin V. Wang[1], Daniel Ruiz[1], Brianna J. Bixler[1], Hannah Linsenbaum[1], Jian-Feng Xiang[1], Samantha Forestier[1], Andrew M. Shafik[1], Peng Jin[1], and Victor G. Corces[1]

SUPLEMENTAL INFORMATION

This file includes

Materials and Methods

Experimental Model and Subject Details

Mice were maintained and handled in accordance with the Institutional Animal Care and Use policies at Emory University. All experiments were conducted according to the animal research guidelines from NIH and all protocols for animal usage were reviewed and approved by the Institutional Animal Care and Use Committee (IACUC). Mice were housed in standard cages on a 12: 12 h light:dark cycle and given ad lib access to food and water. Healthy 8-week-old CD1 mice (Charles River Labs, Raleigh location, unit R09) not involved in previous procedures were used for all experiments.

BPA administration

Gestating females (P0) were administered daily intraperitoneal injections of Bisphenol A (Sigma 239658, 50 mg/kg) or sesame oil (Sigma S3547). Injections were performed from embryonic day 7.5 through 13.5. No sibling breeding was used to avoid inbreeding artifacts. To examine transgenerational transmission of obesity, two pregnant females were exposed to BPA and two additional ones were injected with sesame oil vehicle as controls. Crosses between the F1 progeny of each female were performed as shown in Figure S1A. For each generation, one male and one female with weights equal to the median for the litter arising from each of the original P0 exposed females were crossed, and the crosses were continued as indicated in Figure S1A. This experiment was repeated 7 times by three different investigators. Only two of the experiments were carried out to reach the F7 generation. Numbers of animals used from each generation to perform experiments described in the Results section are listed in the corresponding figure legends. On average, the litter size ranges from 8 to 14 pups (average litter size: 11.7 pups in WT_CTL, 11.5 pups in WT_BPA, 12.3 pups in *Fto*^{c}_CTL and 11.3 pups in *Fto*^{c}_BPA). Pups were eliminated at birth to reach a size of 12 pups when litter sizes were larger than 12 animals. Litter with less than 8 pups were excluded from the experiment. The body weight data shown in Figure 1A is a combination of that obtained in 6 of the experiments performed involving exposure to BPA. Weight data for an additional experiment is shown in Figure 5A. Although the weight of all animals in all experiments was measured, only a subset of weights determined at the specific time points indicated is shown in the figures.

Isolation of mouse sperm and oocytes

Euthanasia was performed by cervical dislocation and the epididymis was removed. Mature sperm were collected from the dissected cauda epididymis of 8-10-week-old CD1 mice. After dissection to eliminate blood vessels and fat, the cauda epididymis was rinsed with PBS, deposited in Donners medium in a cell culture plate, and punctured with a needle. Sperm were then transferred to a tube and allowed to swim up for 1 hr (1). Purity of sperm was determined by examination under a microscope after DAPI staining. After counting 1000 sperm, purity was determined to be at least 99.9% if no contaminating cells were observed (2). Ovaries were harvested from 16-day-old CD1 female pups for the preparation of GV-stage oocytes. The zona pellucida was removed with hyaluronidase to avoid any residual cumulus cells (3).

In vitro fertilization (IVF) and embryo transfer

IVF was performed using BPA-F2 MII oocytes and epididymal sperm from control males. In brief, superovulation was induced in 13 BPA-F2 CD1 females at 6-8 weeks of age using intraperitoneal injection of 7.5 IU of pregnant mare serum gonadotropin (PMSG) followed by 5 IU of human chorionic gonadotropin (hCG) at 48 h post-PMSG injection. MII oocytes were harvested at 13-14 h post-hCG injection. Sperm collected from the cauda epididymis were transferred into droplets containing oocytes. After 3-4 h of co-incubation, oocytes were freed from sperm and cumulus cells using a fine glass pipette. For embryo transfer experiments, two-cell embryos produced by

IVF were transferred into the oviducts of 7 pseudopregnant control CD1 females mated with a vasectomized male. A total of 42 pups were obtained and analyzed as described in the Results.

Targeted deletion of the CTCF binding site in the *Fto* proximal CRE

To generate mice carrying a deletion of the FOXA1 and CTCF binding sites in intron 8 of the *Fto* gene, two clustered regularly interspaced short palindromic repeat (CRISPR) guide RNAs (gRNAs) were designed as shown in Figure S5A. 50 ng/µl of each gRNA and 100 ng/µl of Cas9 RNA were injected into one-cell CD1 zygotes. Embryos were cultured to the 2-cell stage overnight and transferred to pseudopregnant females. After birth, all mice were genotyped by PCR amplification using genomic DNA isolated from mouse tails with PCR primers (5'-CATCAAAGTTGAGCCTCCAAG -3' and 5'- CATCTCAGGAGCCAACAAAGG-3') followed by sequencing of the amplified DNA to verify the targeted deletion. Homozygous mutant mice were isolated using appropriate crosses.

Indirect calorimetry and food intake

Male mice were singly housed in metabolic cages (Columbus Instruments CLAMS-HC) and maintained under otherwise standard housing conditions (12-hour light-dark cycle; 22.2 ± 1.1°C) for indirect calorimetry and food intake assessments. After a 2-day acclimation period, O_2 consumption, CO_2 production, food intake, and activity were monitored over 14-minute periods for consecutive light-dark cycles over 3 successive days. The respiratory exchange ratio (RER) was calculated as the ratio of CO_2 production over O_2 consumption in 14-minute intervals. Time points with artifactual O_2 spikes were excluded. Mice were provided ad libitum food access. Only mice that displayed cyclical eating behavior as shown in cumulative food consumption plots were included for food consumption comparisons. Mice from cages where substantial spikes in food intake activity were measured followed by prolonged eating inactivity were excluded from comparisons. For each mouse, total food intake and Z-counts was averaged per light and dark cycles in which no abnormal activity events occurred. O_2 consumption, CO_2 production, and energy expenditure was normalized by bodyweight in kg.

Analysis of SCA-1 positive cells

Visceral WAT was isolated from male mice and subdivided into 0.2-0.3 cm^3 sized pieces. The tissue sections were incubated in 5 ml 4% paraformaldehyde in PBS for 30 min with gentle rocking on a rotator and then rinsed with PBS three times. The tissues were blocked for 1 h with 5% BSA in PBS at room temperature and then incubated with primary anti-SCA-1 antibody (AB4336 Sigma-Aldrich) overnight at 4°C. The next day, tissues were washed with PBS three times, 10 min per wash and incubated with secondary antibody for 1 h at room temperature. Then slides were mounted with ProLong Gold Antifade Mountant and DAPI (ThermoFisher Scientific) to visualize the nuclei. Percentage of cells positive for SCA-1 was calculated as the ratio to all DAPI stained nuclei. The total number of nuclei counted is WT_CTL n=690, WT_BPA n=767, Fto^c_CTL n=723, Fto^c_BPA n=645.

Measurement of serum leptin

Mice were exsanguinated at time of death by cardiac puncture to collect whole blood. Blood was allowed to clot in microfuge tubes at room temperature for 30 min, and then centrifuged at 1,500 g for 15 min at 4°C to collect serum. Serum leptin levels were assayed using a Millipore mouse leptin ELISA kit (Cat. # EZML-82K) according to the manufacturer's instructions. The sensitivity of the ELISA assay was determined by the manufacturer to be 0.05 ng/ml for a 10 µl sample size, and the intra-assay coefficient of variation was determined to be between 1.06 and 4.59 %.

Adipocyte fluorescence assay and measurement of visceral white adipose tissue

Visceral adipose tissue was fixed for 30 min in 4% paraformaldehyde, washed with PBS, and stained with HCS LipidTox detection reagent (Invitrogen H34476). Stained tissues were then photographed under a Zeiss Axio Observer Z1 microscope. The fraction of visceral white adipose

tissue was calculated using the following formula: [area of fat mass (g)/ whole body weight (g)] x 100.

Assay for transposase-accessible chromatin using sequencing (ATAC-seq)

ATAC-seq was carried out using the Omni-ATAC protocol (4). After sperm cells were counted, the nuclei from 100,000 sperm were isolated with Lysis Buffer (10 mM Tris-HCl pH 7.4, 10 mM NaCl, 3 mM $MgCl_2$) containing 0.1% NP40, 0.1% Tween-20, and 0.01% digitonin. The purified nuclei pellet was then resuspended in the transposase reaction mix containing 0.05% digitonin and incubated for 30 min at 37°C. To perform ATAC-seq using GV oocytes, around 500 oocytes were deposited in a tube with 500 μl of resuspension buffer (10 mM Tris-HCl pH 7.4, 10 mM NaCl and 3 mM $MgCl_2$), and spun down at 500 rcf for 5 min. After careful removal of the supernatant, 15 μl of 2x TD buffer, 0.75 μl of Tn5, 0.3% of 1% Digitonin, 0.3% of 10% Tween 20 and 0.3 μl of 10% NP40, were added and samples were incubated for 30 min at 37°C. Following incubation, nuclei were treated with Proteinase K at 55°C for 2 h, and gDNA was isolated by phenol:chloroform:isoamyl alcohol and EtOH precipitation. Library amplification was done with 2x KAPA HiFi mix (Kapa Biosystems) and 1.25 μM indexed primers using the following PCR conditions: 72°C for 5 min; 98°C for 30 s; 10-11 cycles at 98°C for 10 s, 63°C for 30 s, and 72°C for 1 min. Two independent biological replicates from two different mice were paired-end sequenced on Illumina Hiseq2500 v4 or NovaSeq 6000 instruments.

Bisulfite Sanger sequencing

DNA was extracted from epididymal sperm using phenol/chloroform/isoamylalcohol (25:24:1). About 2 μg of DNA was bisulfite converted and purified using the Zymo EZ DNA methylation lightning kit (D5030) following the manufacturer's protocol. Bisulfite converted DNA was then used as template for PCR amplification with KAPA HiFi HotStart Uracil kit (Roche, KK2801) using primers surrounding Site 1 in intron 8 of the *Fto* gene. The resulting 470 bp fragment was purified using the Zymoclean Gel DNA Recovery kit (D4008). Primer sequences used were as follows: forward 5'- TGGAGTAGGYGTTTTGAGGTGAAAGGGTAG-3' and reverse, 5'- TCACTACRATTTTTCCTAACATAACAAAC-3'. Amplicons were ligated to T-Vector pMD19 (Takara, No.3271) with T4 ligase (NEB, M0202L) and transformed into DH-5α competent cells. DNA was isolated from monoclonal bacterial colonies and sequenced.

Whole genome bisulfite sequencing

DNA (1~2 μg) was isolated from cauda epididymis sperm using phenol:chloroform:isoamyl alcohol followed by EtOH precipitation and spiked with 0.5% unmethylated lambda genomic DNA (Promega) to determine conversion efficiency after bisulfite treatment. The DNA was sheared with a Diagenode Bioruptor to yield DNA fragments ranging from 200 to 500 bp. After purification of the fragmented DNA using phenol/chloroform, DNA fragments were end repaired, A-tailed, and ligated to methylated Illumina adaptors. The Zymo EZ DNA methylation lightning kit (D5030) was used for bisulfite conversion and subsequent purification according to the manufacturer's instructions. Two independent biological replicates per sample were then sequenced using paired-end 50 bp on Illumina Hiseq2500 v4 or NovaSeq 6000 instruments.

ChIP-seq

Sperm were crosslinked with 1% formaldehyde in PBS for 10 min at room temperature (RT) and the reaction was quenched with 125 mM glycine for 10 min at RT. After washing with PBS, cells were lysed with 5 mM PIPES pH 6.9, 85 mM KCl, 0.5% NP40 and 1x protease inhibitors (P8107S, NEB) on ice for 15 min. After centrifugation, cells were resuspended in RIPA buffer (1x PBS; 1% NP40; 0.5% sodium deoxycholate; 0.1% SDS; 1x protease inhibitors) and incubated on ice for 20 min. The purified chromatin was sonicated to 300-500 bp using a Diagenode Bioruptor. After 25 cycles (30 s on and 60 s off), the supernatant containing sheared chromatin was collected. Immunoprecipitation was performed overnight at 4°C with CTCF antibodies (#3418, Cell Signaling

Technology). Libraries for Illumina sequencing were constructed using the following standard protocol. Fragment ends were repaired using the NEBNext End Repair Module and adenosine was added at the 3' ends using Klenow fragment (3' to 5' exo minus, New England Biolabs). Precipitated DNA was incubated with adaptors at room temperature for 1 h with T4 DNA ligase (New England Biolabs) and amplified with Illumina primers. Two independent biological replicates per sample were then sequenced using paired-end 50 bp on an Illumina NovaSeq 6000 instrument.

RNA-seq

Total RNA was isolated from epididymal sperm using Trizol reagent (Invitrogen) and ribosomal RNA was removed using the RiboMinus Transcriptome isolation kit (Invitrogen, K1550). RNA concentration was measured using the Qubit RNA HS Assay kit (Thermo Fisher) and fragmented randomly by adding fragmentation buffer. cDNA was synthesized using the RNA template and random hexamer primers. After terminal repair, A ligation, and sequencing adaptor ligation, the double-stranded cDNA library was completed by size selection and PCR enrichment. Two independent biological replicates per sample were then sequenced using paired-end 50 bp on an Illumina NovaSeq 6000 instrument.

MeRIP-seq

Total RNA from sperm was isolated as described above. For m^6A immunoprecipitation, purified RNA was digested using RNA Fragmentation Reagents (Ambion AM8740) by incubation at 70°C for 5 min in fragmentation buffer and precipitated via standard ethanol precipitation. Anti-m^6A antibody (Synaptic Systems Cat.no 202 003) was incubated with 30 μl of Dynabeads Protein A for 1 h at 4°C. Fragmented RNA was incubated with the antibody-bead mixture overnight at 4°C. Library preparation was performed using the SMARTer Stranded Total RNA-seq kit v2 (Takara) according to the manufacturer's protocol. Two independent biological replicates per sample were then sequenced using paired-end 50 bp on an Illumina NovaSeq 6000 instrument.

Chromosome-associated RNA m^6A-seq

Fractionation of chromosome-associated RNAs and generation of m^6A-seq libraries were carried out as described(5). Briefly, 10^8 sperm cells were isolated from the cauda epididymis and resuspended in cold lysis buffer (10 mM Tris-HCl pH 7.4, 0.05% NP40, 150 mM NaCl). After incubation on ice for 5 min, cells were resuspended in 2.5 volumes of sucrose solution (24% sucrose in lysis buffer), and then centrifuged at 4°C at 14,000 g for 10 min. The supernatant containing the cytoplasmic fraction was removed and the nuclei pellet was resuspended in glycerol buffer (20 mM Tris-HCl pH 7.4, 75 mM NaCl, 0.5 mM EDTA, 0.85 mM DTT, 0.125 mM PMSF, 50% glycerol) and an equal volume of cold nuclei lysis buffer (10 mM HEPES pH 7.0, 10 mM DTT, 7.5 mM $MgCl_2$, 0.2 mM EDTA, 0.3 M NaCl, 1 M urea, 1% NP40). After resuspending the pellet by vortexing, the nuclei were incubated on ice for 2 min and centrifuged at 4°C at 14,000 g for 2 min. The supernatant containing the soluble nuclear fraction/nucleoplasm was removed and the chromosome-associated fraction was collected in the pellet. Total RNA from the chromosome-associated fraction was isolated with Trizol. Ribosomal RNA was removed using the RiboMinus transcriptome isolation kit (Invitrogen, K1550), and then RNA was digested using RNA Fragmentation Reagents (Ambion AM8740) by incubation at 70°C for 5 min. m^6A-immunoprecipitaion was performed using the EpiMark N6-Methyladenosine Enrichment Kit (NEB E1610S), followed by library preparation using the SMARTer Stranded Total RNA-seq kit v2 (Takara) according to the manufacturer's protocols. Two independent biological replicates per sample were then sequenced using paired-end 50 bp on an Illumina NovaSeq 6000 instrument.

***In-situ* Hi-C**

In-situ Hi-C libraries were prepared using DpnII restriction enzyme as previously described (6). Briefly, 10 million sperm were crosslinked with 1% formaldehyde, quenched with glycine, washed

with PBS, and permeabilized to obtain intact nuclei. Nuclear DNA was then digested with DpnII, the 5'-overhangs were filled with biotinylated dCTPs and dA/dT/dGTPs to make blunt-end fragments, which were then ligated, reverse-crosslinked, and purified by standard DNA ethanol precipitation. Purified DNA was sonicated to 200-500 bp fragments and captured with streptavidin beads. Standard Illumina TruSeq library preparation steps, including end-repairing, A-tailing, and ligation with universal adaptors were performed on beads, washing twice in Tween Washing Buffer (5 mM Tris-HCl pH 7.5, 0.5 mM EDTA, 1 M NaCl, 0.05% Tween 20) between each step. DNA on the beads was PCR amplified with barcoded primers using KAPA SYBR FAST qPCR Master Mix (Kapa Biosystems) for 5~12 PCR cycles to obtain enough DNA for sequencing. Libraries were paired-end sequenced on an Illumina NovaSeq 6000 instrument. Two biological replicates were generated, and replicates were combined for all analyses after ensuring high correlation.

Analysis of ATAC-seq data

Paired reads were aligned to the mouse mm10 reference genome using Bowtie2 (7). ATAC-seq reads were aligned using default parameters except -X 2000 -m 1. PCR duplicates were removed using Picard Tools (http://picard.sourceforge.net; https://broadinstitute.github.io/picard/). To adjust for fragment size, we aligned all reads as + strands offset by +4 bp and – strands offset by -5 bp (8). For all ATAC-seq datasets subnucleosome size and mono-nucleosome-size reads were separated by choosing fragments 50-115 bp and 180-247 bp in length, respectively. MACS2(9) was used for peak calling of subnucleosomal reads, which represent bound transcription factors. Bedgraph files were converted into bigwig by using bedGraphToBigWig. DiffBind was used to identify differential ATAC-seq peaks between control and BPA-treated samples with a cut-off p value ≤0.05 and fold change ≥2. To identify transcription factor binding motifs, we analyzed a region from -50 bp to +50 bp with respect to the summits of ATAC-seq peaks. We used motif information from the JASPAR database (10) along with the Find Individual Motif Occurrences (FIMO) algorithm from the MEME Suite (11).

ChIP-seq data processing

All reads were mapped to unique genomic regions using Bowtie2 (7) and the mm10 mouse genome. PCR duplicates were removed using Picard Tools (http://picard.sourceforge.net; https://broadinstitute.github.io/picard/). MACS2 (9) was used to call peaks using default parameters with IgG ChIP-seq data as a control.

Analysis of BS-seq data

Paired-end reads 50 bp were trimmed with Trimmomatic-0.38 to remove low quality sequence and any remnant adaptor sequence (12). The trimmed reads were aligned to the bisulfite converted mm10 mouse genome using aligner (v0.21) with default parameters (13). Duplicate reads were removed with Bismark Deduplicate, and then Bismark Methylation Extractor provides final methylation percentages per each CpG site (coverage ≥5). Two biological replicates for each condition were processed and merged for analysis.

RNAseq data processing

The raw RNA-sequencing reads were filtered by FastQC (14), and all reads were aligned using STAR (v-2.7.1) to the mm10 mouse genome with default parameters. Differentially expressed genes were identified using the R package "Deseq2" with a cut-off *p* value ≤0.05 and fold change ≥2 (15).

MeRIP-seq and chromosome-associated RNA m^{6}A-seq data analysis

Raw reads were trimmed with Trimmomatic-0.38, then aligned to the mouse genome and transcriptome (mm10) using transcriptome-based aligner HISAT2 (version 2.2.0) with '--rna-strandness RF' parameters (16). Annotation files downloaded from the GENCODE database

(https://www.gencodegenes.org/) were used. m^6A peaks were called using MACS with parameter '--nomodel' and '--keep-dup 5'. For differential peak analysis, the R package "DiffBind" was used and m^6A peaks were considered to be significantly different with an absolute fold change >2 and FDR <0.05 (17).

Hi-C data processing

Paired-end reads from Hi-C experiments were aligned to the mouse mm10 reference genome using Juicer (6). After PCR duplicates and low-quality reads were removed, high-quality reads were assigned to DpnII restriction fragments, and Hi-C interaction contacts were mapped in a binned matrix to create hic files that contain the unnormalized Hi-C signal. Fit-Hi-C (18) was used to call significant interaction pairs at 25 kb resolution with a q-value threshold of q > 0.001. SIP was used to obtain distance-normalized Hi-C signals (value-normalized = 1 + ((value − expected)/expected + 1)) for each Fit-Hi-C significant interaction (19). The resulting distance normalized matrices for all significant interaction were then subjected to downstream analysis. The average distance-normalized Hi-C signal was analyzed using SIPmeta bullseye transformed metaplot (19), and only significant Hi-C interactions with at least one anchor overlapping with the proximal and/or distal *Fto* CREs were included (31 and 10 significant interactions for proximal and distal CREs, respectively). The plot connections function in the Cicero package (20) was used to obtain arc views of significant interactions using proximal and/or distal *Fto* CREs as viewpoints, and the differences of distance normalized score in all significant interaction between BPA-F3 and CTL were analyzed.

Statistical Analyses of Metabolic Data

The Shapiro-Wilk test was used to assess the normality of the data. Two-tailed t-tests were used when comparing two groups with normally distributed data. One-way ANOVA was used when comparing the body weights of more than three groups at only one time point. Dunnett's multiple comparison post-hoc test was used when comparing each group with the control group when appropriate. Tukey's multiple comparison post-hoc test was used when comparing each group with every other group when appropriate. We performed individual t-tests to compare the bodyweights of mice of the same age that were ancestrally exposed to different BPA concentrations against the control group without correcting for multiple comparisons. We used the Kruskal-Wallis tests when comparing bodyweights from parental outcross experiments and IVF experiments with their respective controls, since the controls for these experiments were not normally distributed. We corrected for multiple comparisons by controlling the False Discovery Rate with the original Benjamini and Hochberg method. When comparing RER or bodyweight of groups over time, we analyzed the data by fitting a mixed model as implemented in GraphPad Prism 9.3, which allows values missing at random, and can be interpreted like a repeated measures ANOVA. This mixed model uses a compound symmetry covariance matrix and is fit using Restricted Maximum Likelihood (REML). Šidák's multiple comparison post-hoc test was used to assess the time points at which body weights were significantly different. Welch's t-tests were used to compare serum leptin levels between controls and BPA mice within different ages. Holm-Šidák method was used to correct for multiple testing. Two-way ANOVA for repeated measures was used to analyze differences in average food consumption, RER, and energy expenditure during the light and dark cycles between control and treatment groups. Šidák's multiple comparison post-hoc test was used where applicable. All analyses were performed on GraphPad Prism 9.3.

Supplemental Figures and Tables

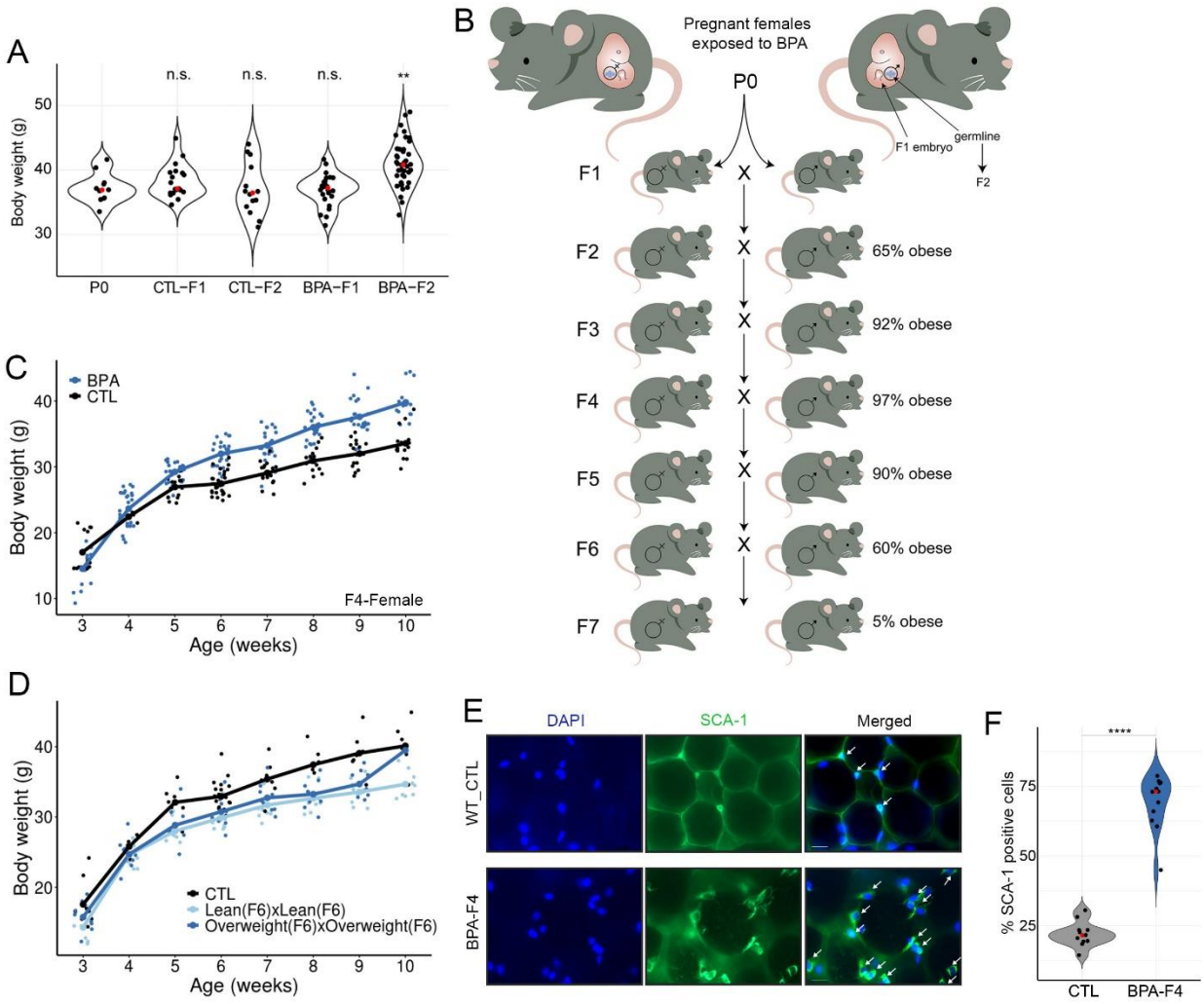

Figure S1. Exposure of pregnant females to BPA causes obesity that can be transmitted transgenerationally. Related to Figure 1.

(A) Changes in body weight between the male progeny of P0 mice injected with sesame oil vehicle (CTL) and the progeny of P0 females injected with 50 mg/kg/day of BPA in sesame oil (BPA). Weights were measured at 10 weeks of age. F1 and F2 progeny were obtained as described in Figure S1B.

(B) In each exposure experiment, two different pregnant CD1 females (P0, which indicates the parental generation, zero) were injected with BPA during days E7.5-E13.5 of embryonic development when the germline of the embryo (labeled in blue) is undergoing demethylation. One male and one female F1 progeny of median weight from each P0 female are crossed to obtain the F2 generation, which arises from the BPA-exposed germline. One F2 male and one F2 female of median weight are crossed to obtain F3, which is the first generation whose cells were not directly exposed to BPA. The percentage of obese mice in each generation is indicated. Obese is defined as having a weight higher than the mean plus one standard deviation of the weights of control mice (see Figure 1B).

(C) Changes in body weight of BPA-F4 females with time (CTL n=16, BPA n=17).

(D) Changes in body weight with time for control and F7 males arising from crosses between BPA-F6 lean or BPA-F6 overweight animals (CTL n=7, Lean (F6) x Lean (F6) n=8, Overweight (F6) x Overweight (F6) n=9).
(E) Immunofluorescence microscopy of visceral fat tissue from control and BPA-F4 mice stained with antibodies to SCA-1, which labels several cell types including adipocyte progenitor cells.
(F) Fraction of SCA-1 positive cells present in the visceral fat tissue of control and BPA-F4 mice (CTL n=12, BPA n=13). P values were calculated as indicated in the Statistical Analyses of Metabolic Data section of Methods; **** $p<0.0001$, ***$p<0.001$, ** $p<0.01$, *$p<0.05$, ns not significant.

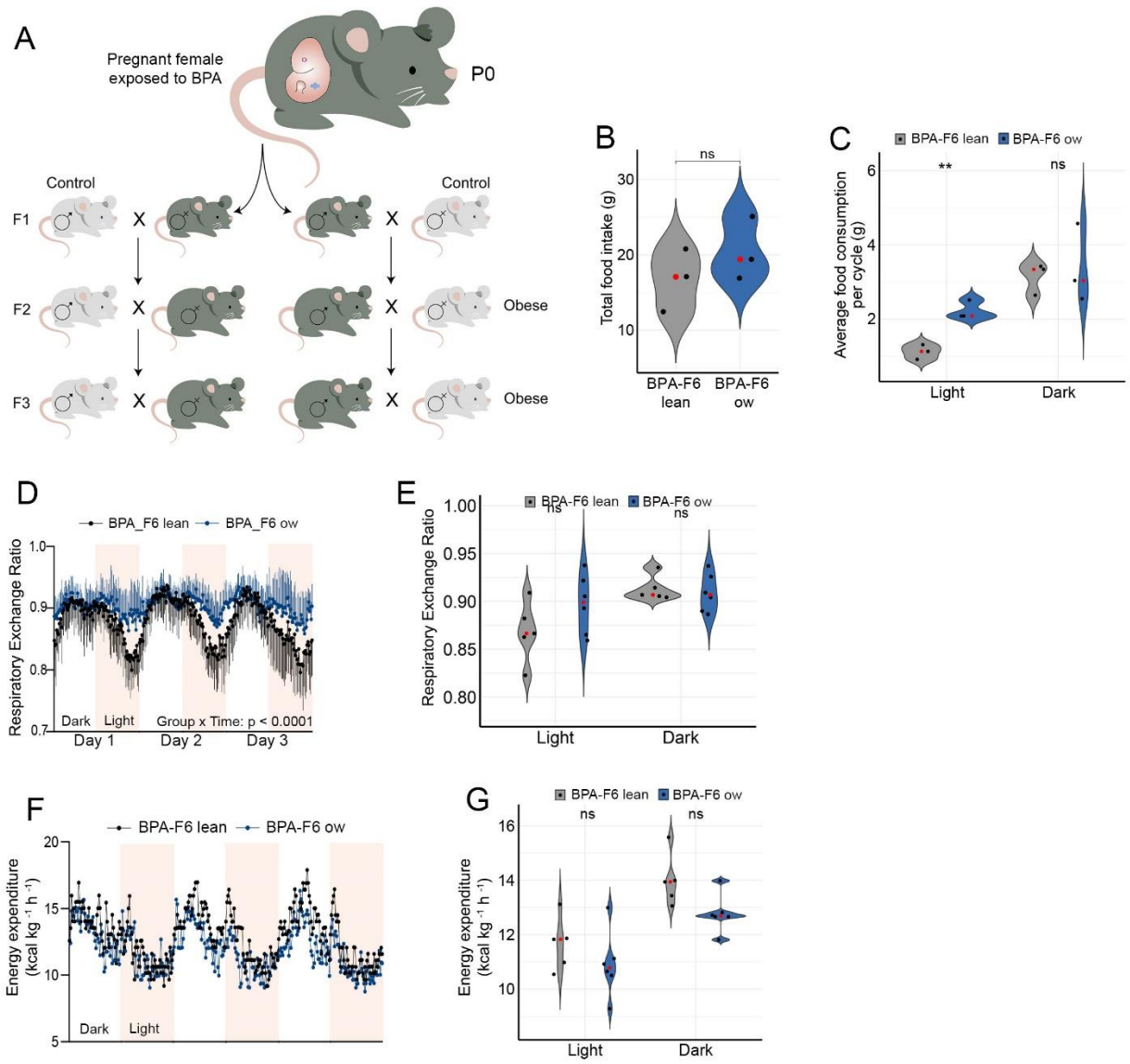

Figure S2. Transgenerational effects of BPA on body weight. Related to Figure 2.
(A) Outcrosses between BPA-F1 males or females and control mice of the opposite sex.
(B) Differences in total daily food intake between control and BPA-F4 males (CTL n=7, BPA n=8).
(C) Average food consumption over a 3-day period during the light and dark cycles in control and BPA-F6 overweight and lean males (BPA-F6 lean n=3, overweight n=3).
(D) Respiratory exchange ratio in a three-day period during the light and dark cycles in BPA-F6 overweight and lean males (BPA-F6 lean n=5, ow n=6).
(E) Cumulative respiratory exchange ratio during the light and dark cycles in BPA-F6 overweight and lean males (BPA-F6 lean n=5, ow n=6).
(F) Energy expenditure over a 3-day period during the light and dark cycles in BPA-F6 overweight and lean males (BPA-F6 lean n=5, overweight n=6).
(G) Cumulative energy expenditure during the light and dark cycles in BPA-F6 overweight and lean males (BPA-F6 lean n=5, overweight n=6). P values were calculated as indicated in the Statistical Analyses of Metabolic Data section of Methods; **** p<0.0001, ***p<0.001, ** p<0.01, *p<0.05, ns not significant.

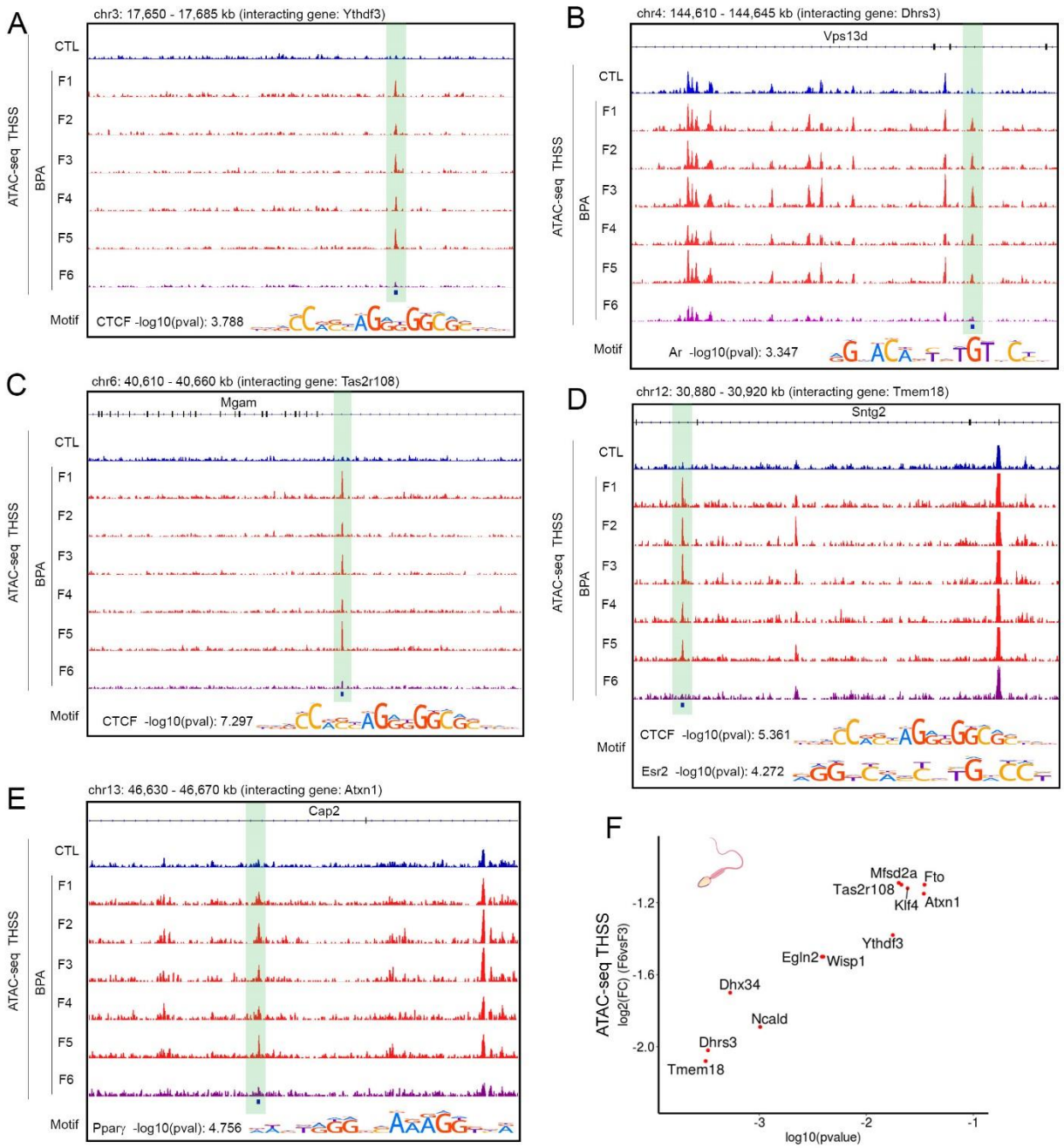

Figure S3. Examples of ATAC-seq sites present in sperm of BPA-F1-F5 but absent in BPA-F6 and control males. Related to Figure 3.

(A) Example of one of the 12 ATAC-seq sites present in an intergenic region; this site contains a CTCF motif, and it preferentially contacts the promoter of the *Ythdf3* gene.

(B) Example of an ATAC-seq site present in a gene intron. This site contains a binding motif for AR. Rather than interacting preferentially with the promoter of the gene in which it is located, the site located in an intron of *Vps13d* interacts with the *Dhrs3* gene.

(C) Example of a second ATAC-seq site present in a gene intron. This site contains a binding motif for CTCF located in an intron of *Mgam* and preferentially interacts with the promoter of *Tas2r108*.

(D) Example of an ATAC-seq site containing binding motifs for CTCF and ESR2 located in an intron of *Sntg2* that interacts with the *Tmem18* gene.
(E) Example of an ATAC-seq site containing a binding motif for Pparγ located in an intron of *Cap2* that preferentially interacts with the promoter of *Atxn*.
(F) Summary of genes whose promoters are contacted with the highest frequency by the 12 ATAC-seq sites present in BPA-F1-F5 but not BPA-F6 or controls based on significant interactions determined by Fit-Hi-C using Hi-C data obtained in sperm of BPA-F3 and CTL-F3 mice. The X-axis indicates the ATAC-seq signal difference between BPA-F3 and BPA-F6, and Y-axis represent the significance of the peaks (log10 *p*-value).

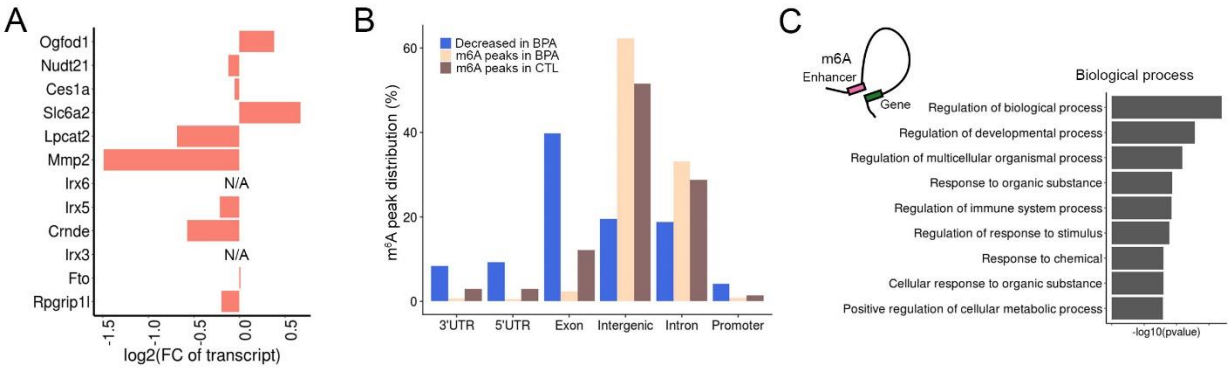

Figure S4. Effect of BPA-induced epigenetic alterations in *Fto* on m^{6}A levels in sperm RNAs. Related to Figure 4.

(A) relative RNA levels in sperm of BPA-F3 and control transcribed from genes present in the region surrounding *Fto*.

(B) Location of sites in RNAs modified by m^{6}A with respect to genomic features.

(C) Biological processes involving genes whose promoters are contacted by enhancers whose eRNAs show decreased levels of m^{6}A in BPA-F3 with respect to control.

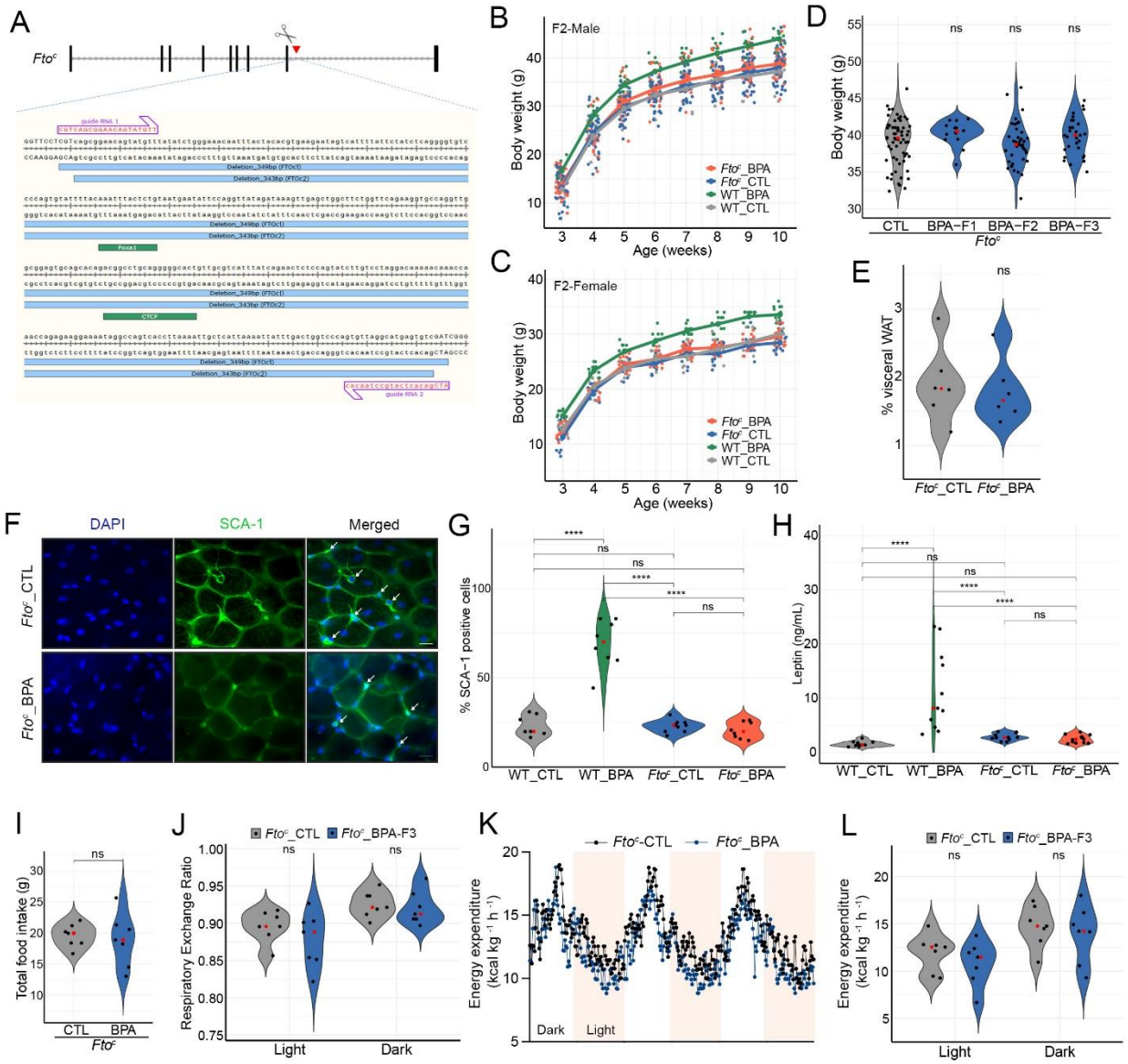

Figure S5. Effect of BPA exposure in mice carrying the *Fto*^{c} allele. Related to Figure 5.
(A) Region of intron 8 of the *Fto* gene containing the FOXA1 and CTCF sites deleted in *Fto*^{c} mice. Two slightly different deletions gave the same results in all analyses.
(B) Weight gain with age of F2 *Fto*^{c} male mice ancestrally exposed to BPA (*Fto*^{c}_CTL n=35, *Fto*^{c}_BPA n=39, WT_CTL n=13, WT_BPA n=14). There is no statistically significant difference between *Fto*^{c}_CTL and *Fto*^{c}_BPA (p=0.18).
(C) Weight gain with age of F2 *Fto*^{c} female mice ancestrally exposed to BPA (*Fto*^{c}_CTL n=11, *Fto*^{c}_BPA n=15, WT_CTL n=15, WT_BPA n=13). There is no statistically significant difference between *Fto*^{c}_CTL and *Fto*^{c}_BPA (p=0.2).
(D) Differences in body weight at 10 weeks of age among unexposed and exposed *Fto*^{c} males from different generations.
(E) Percentage of visceral fat with respect to body weight in 10-week-old *Fto*^{c} male mice of the F3 generation ancestrally exposed or non-exposed to BPA (*Fto*^{c}_CTL n=6, *Fto*^{c}_BPA n=6).
(F) Immunofluorescence microscopy of visceral fat tissue from BPA-exposed and unexposed F3 *Fto*^{c} mice stained with antibodies to SCA-1, which labels several cell types including adipocyte progenitor cells.

(G) Fraction of SCA-1 positive cells present in the visceral fat tissue of WT ancestrally exposed and unexposed F3 males and *Fto*^{c} ancestrally exposed and unexposed F3 males (WT_CTL n=7, WT_BPA n=8, *Fto*^{c}_CTL n=9, *Fto*^{c}_BPA n=8).
(H) Circulating leptin levels in serum of 10-weeks-old male mice from WT ancestrally exposed and unexposed F3 males and *Fto*^{c} ancestrally exposed and unexposed F3 males (WT_CTL n=10, BPA n=11, *Fto*^{c}_CTL n=12, *Fto*^{c}_BPA n=12).
(I) Total food intake by F3 *Fto*^{c} mice ancestrally exposed to BPA and unexposed controls (*Fto*^{c}_CTL n=7, *Fto*^{c}_BPA n=7).
(J) Respiratory exchange ratio, which measures consumption of stored fats versus carbohydrates from a recent meal, is the same in 10-weeks-old F3 *Fto*^{c} mice ancestrally exposed to BPA and unexposed controls (*Fto*^{c}_CTL n=7, *Fto*^{c}_BPA n=7).
(K) Energy expenditure over a 3-day period during the light and dark cycles by 10-weeks-old F3 *Fto*^{c} mice ancestrally exposed to BPA and unexposed controls (*Fto*^{c}_CTL n=7, *Fto*^{c}_BPA n=7).
(L) Cumulative average energy expenditure during the light and dark light cycles by 10-weeks-old F3 *Fto*^{c} mice ancestrally exposed to BPA and unexposed controls (*Fto*^{c}_CTL n=7, *Fto*^{c}_BPA n=7).
P values were calculated as indicated in the Statistical Analyses of Metabolic Data section of Methods; **** $p<0.0001$, ***$p<0.001$, ** $p<0.01$, *$p<0.05$, ns not significant.

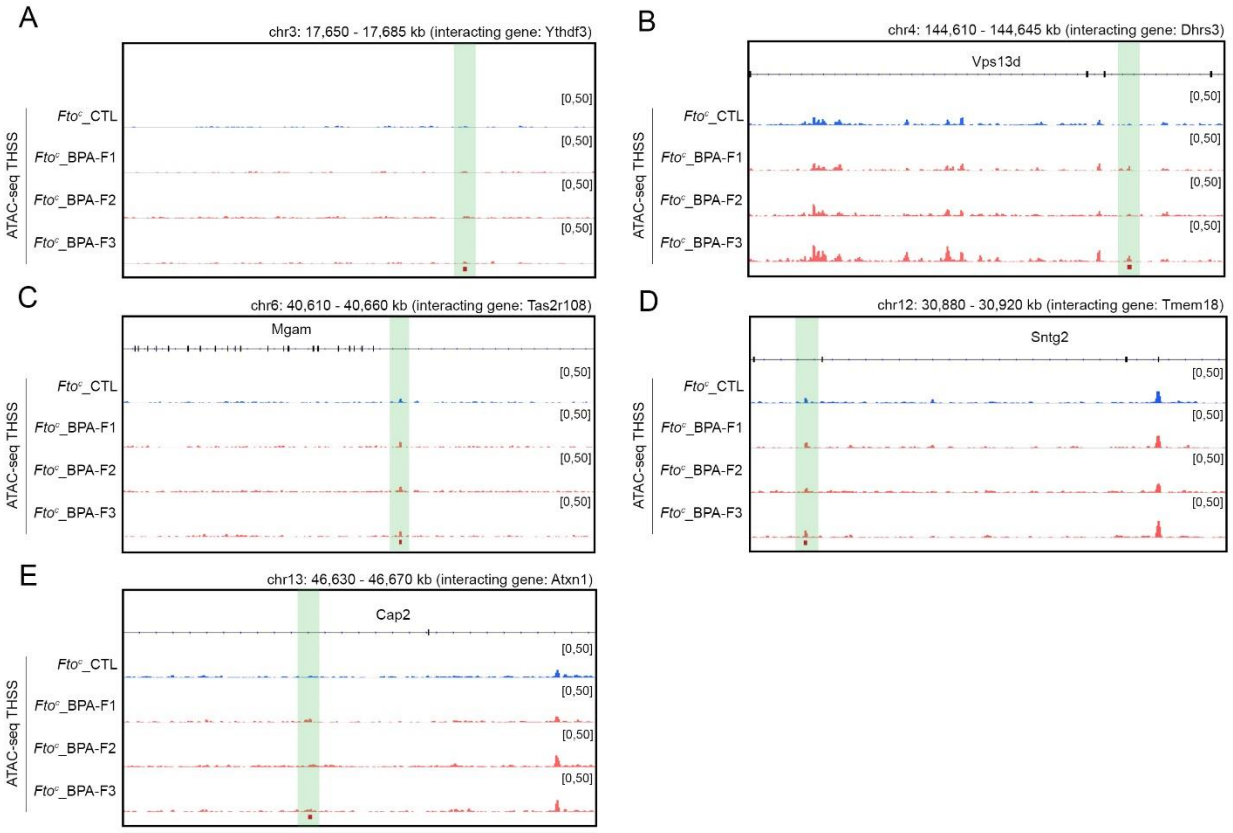

Figure S6. Exposure of *Fto*^{c} mice to BPA fails to induce changes in chromatin accessibility at specific loci. Related to Figure 5. The figure shows the same genomic locations displayed in Figure S3, which contains information for changes in chromatin accessibility in WT mice unexposed and ancestrally exposed to BPA.

(A) Example of an ATAC-seq site present in an intergenic region and containing a CTCF motif. Chromatin accessibility fails to increase after BPA exposure of *Fto*^{c} mice (compare with results in WT mice shown in Figure S3A).

(B) Example of an intronic ATAC-seq site containing a binding motif for AR (compare to Figure S3B).

(C) Example of a second ATAC-seq site present in a gene intron and containing a binding motif for CTCF (compare to Figure S3C).

(D) Example of an ATAC-seq site contain binding motifs for CTCF and ESR2 located in an intron of *Sntg2* (compare to Figure S3D).

(E) Example of an ATAC-seq site contain a binding motif for PPARγ located in an intron of *Cap2* (compare to Figure S3E).

Supplemental Tables

	BPA_sperm_HiC_Rep1	BPA sperm_HiC_Rep2
Sequenced Read Pairs	2,233,501,205	1,213,338,046
Normal Paired	1,990,429,856 (89.12%)	958,754,384 (79.02%)
Chimeric Paired	639,944 (0.03%)	77,090 (0.01%)
Chimeric Ambiguous	515,747 (0.02%)	100,754 (0.01%)
Unmapped	241,915,658 (10.83%)	254,405,818 (20.97%)
Ligation Motif Present	580,866,418 (26.01%)	761,588,883 (62.77%)
Alignable (Normal+Chimeric Paired)	1,991,069,800 (89.15%)	958,831,474 (79.02%)
Unique Reads	740,243,549 (33.14%)	796,355,330 (65.63%)
PCR Duplicates	832,816,127 (37.29%)	157,435,772 (12.98%)
Optical Duplicates	410,653,520 (18.39%)	5,040,372 (0.42%)
Library Complexity Estimate	894,223,071	2,561,626,782
Intra-fragment Reads	84,879,076 (3.80% / 11.47%)	30,467,531 (2.51% / 3.83%)
Below MAPQ Threshold	311,738,906 (13.96% / 42.11%)	284,663,928 (23.46% / 35.75%)
Hi-C Contacts	343,625,567 (15.39% / 46.42%)	481,223,871 (39.66% / 60.43%)
Ligation Motif Present	85,483,246 (3.83% / 11.55%)	270,101,845 (22.26% / 33.92%)
3' Bias (Long Range)	87% - 13%	94% - 6%
Pair Type %(L-I-O-R)	25% - 25% - 25% - 25%	25% - 25% - 25% - 25%
Inter-chromosomal	94,037,833 (4.21% / 12.70%)	124,186,443 (10.24% / 15.59%)
Intra-chromosomal	249,587,734 (11.17% / 33.72%)	357,037,428 (29.43% / 44.83%)
Short Range (<20Kb)	113,196,712 (5.07% / 15.29%)	137,765,772 (11.35% / 17.30%)
Long Range (>20Kb)	136,384,593 (6.11% / 18.42%)	219,267,003 (18.07% / 27.53%)

Table S1. Quality control and mapping statistics of Hi-C libraries

Chrom	Start	End	Closest gene	Interacting genes	Protein Function
chr3	17675248	17675548	Ythdf3	Ythdf3	m6A binding protein
chr4	56698064	56698364	Klf4	Klf4	Transcription factor
chr4	121054176	121054476	Cap1	Ppt1	Palmitoyl-protein thioesterase 1
				Mfsd2a	Sodium-dependent lysophosphatidylcholine (LPC) symporter; involved in the establishment of the blood-brain barrier and is required for brain growth and function
chr4	144637916	144638216	Vps13d	Dhrs3	Endoplasmic reticulum protein associated with lipid droplet accumulation
chr6	40639252	40639552	Mgam	Tas2r108	Tas2 receptor
chr7	16792929	16793229	Dhx34	Dhx34	DEAD box RNA helicase
				C5ar1 and C5ar2	Complement receptor
				Nova2	Regulator of alternative splicing
				Nanos2	RNA binding protein involved in germcell differentiation
				Dmpk	Non-receptor serine/threonine protein kinase which is necessary for the maintenance of skeletal muscle structure and function
				Six5	Transcription factor involved in organogenesis
				Qpctl	Glutaminyl-Peptide Cyclotransferase Like
				Gipr	G-protein coupled receptor for gastric inhibitory polypeptide (GIP) demonstrated to stimulate insulin release in the presence of elevated glucose.
				Ercc1	Nucleotide excision repair pathway
				Ppp1r13l	Protein Phosphatase 1 Regulatory Subunit 13 Like
chr7	26612262	26612562	Cyp2s1	Egln2	
chr8	94055911	94056211	Fto	Fto	m6A RNA demethylase
				Rpgrip1l	Retinitis pigmentosa GTPase regulator-interacting protein 1 like; critical for the function of the primary cilium
				Irx3	Iroquois family homeobox transcription factor
				Irx5	Iroquois family homeobox transcription factor
				Mmp2	Matrix metalloproteinase-2
				Slc6a2	Solute carrier family 6 member 2
chr12	30884640	30884940	Sntg2	Tmem18	Inhibits osteogenic differentiation of mesenchymal stem cells; controls apetite and body weight; is located in the nuclear membrane and binds DNA in a sequence-specific manner; Tmem18 deficiency in mice results in a higher body weight owing to increased food intake, whereas Tmem18 overexpression reduces food intake and limits weight gain
				Myt1L	Transcription factor involved in neural differentiation represses non-neuronal genes; expressed in brain only; altered development of the neuroendocrine hypothalamus; associated with obesity and intellectual disability
chr13	46645735	46646035	Cap2	Rmb24	RNA binding protein; represses p53 translation
				Atxn1	Spinocerebellar Ataxia Type 1 Protein
chr15	37772738	37773038	Ncald	Ncald	Neurocalcin-delta is a potential memory-related factor in the hippocampus of obese rats induced by high-fat diet
chr15	66781782	66782082	Ndrg1	Thyroglobulin	Thyroid hormone
				Wisp 1	Downstream regulator in the Wnt/Frizzled-signaling pathway

Table S2. Description of the roles of genes contacted by the 12 ATAC-seq sites present in sperm of BPA-F1-F5 but absent in sperm of BPA-F6 and control males.

Supplemental References

1. M. Hisano *et al.*, Genome-wide chromatin analysis in mature mouse and human spermatozoa. *Nat Protoc* **8**, 2449-2470 (2013).
2. Y. H. Jung *et al.*, Chromatin States in Mouse Sperm Correlate with Embryonic and Adult Regulatory Landscapes. *Cell Rep* **18**, 1366-1382 (2017).
3. Y. H. Jung *et al.*, Maintenance of CTCF- and Transcription Factor-Mediated Interactions from the Gametes to the Early Mouse Embryo. *Mol Cell* **75**, 154-171 e155 (2019).
4. M. R. Corces *et al.*, An improved ATAC-seq protocol reduces background and enables interrogation of frozen tissues. *Nat Methods* **14**, 959-962 (2017).
5. J. Liu *et al.*, N (6)-methyladenosine of chromosome-associated regulatory RNA regulates chromatin state and transcription. *Science* **367**, 580-586 (2020).
6. S. S. Rao *et al.*, A 3D map of the human genome at kilobase resolution reveals principles of chromatin looping. *Cell* **159**, 1665-1680 (2014).
7. B. Langmead, S. L. Salzberg, Fast gapped-read alignment with Bowtie 2. *Nat Methods* **9**, 357-359 (2012).
8. J. D. Buenrostro, P. G. Giresi, L. C. Zaba, H. Y. Chang, W. J. Greenleaf, Transposition of native chromatin for fast and sensitive epigenomic profiling of open chromatin, DNA-binding proteins and nucleosome position. *Nat Methods* **10**, 1213-1218 (2013).
9. T. Liu, Use model-based Analysis of ChIP-Seq (MACS) to analyze short reads generated by sequencing protein-DNA interactions in embryonic stem cells. *Methods Mol Biol* **1150**, 81-95 (2014).
10. O. Fornes *et al.*, JASPAR 2020: update of the open-access database of transcription factor binding profiles. *Nucleic Acids Res* **48**, D87-D92 (2020).
11. T. L. Bailey, J. Johnson, C. E. Grant, W. S. Noble, The MEME Suite. *Nucleic Acids Res* **43**, W39-49 (2015).
12. A. M. Bolger, M. Lohse, B. Usadel, Trimmomatic: a flexible trimmer for Illumina sequence data. *Bioinformatics* **30**, 2114-2120 (2014).
13. F. Krueger, S. R. Andrews, Bismark: a flexible aligner and methylation caller for Bisulfite-Seq applications. *Bioinformatics* **27**, 1571-1572 (2011).
14. J. Brown, M. Pirrung, L. A. McCue, FQC Dashboard: integrates FastQC results into a web-based, interactive, and extensible FASTQ quality control tool. *Bioinformatics* **33**, 3137-3139 (2017).
15. H. Varet, L. Brillet-Gueguen, J. Y. Coppee, M. A. Dillies, SARTools: A DESeq2- and EdgeR-Based R Pipeline for Comprehensive Differential Analysis of RNA-Seq Data. *PLoS One* **11**, e0157022 (2016).
16. D. Kim, J. M. Paggi, C. Park, C. Bennett, S. L. Salzberg, Graph-based genome alignment and genotyping with HISAT2 and HISAT-genotype. *Nat Biotechnol* **37**, 907-915 (2019).
17. R. Stark, G. Brown, DiffBind: differential binding analysis of ChIP-Seq peak data. http://bioconductor.org/packages/release/bioc/vignettes/DiffBind/inst/doc/DiffBind.pdf (2011).
18. F. Ay, T. L. Bailey, W. S. Noble, Statistical confidence estimation for Hi-C data reveals regulatory chromatin contacts. *Genome Res* **24**, 999-1011 (2014).
19. M. J. Rowley *et al.*, Analysis of Hi-C data using SIP effectively identifies loops in organisms from C. elegans to mammals. *Genome Res* 10.1101/gr.257832.119 (2020).
20. H. A. Pliner *et al.*, Cicero Predicts cis-Regulatory DNA Interactions from Single-Cell Chromatin Accessibility Data. *Mol Cell* **71**, 858-871 e858 (2018).